GRB Scaler Data Analysis using the Milagro Detector

A Thesis Submitted in Partial Satisfaction
of the Requirements for the Degree of
Bachelor of Science in Physics(Astrophysics)
at the
University of California, Santa Cruz

by

Eitan Anzenberg

June 2006

_____	_____
David A. Williams	Clemens Heusch
Technical Advisor	Supervisor of Senior Theses, 2005-2006

_____
David Belanger
Chair, Department of Physics

Abstract

The Milagro experiment is a 5000 m^2 water Cherenkov detector used for high energy gamma-ray astronomy, specifically for the detection of Gamma-ray Bursts (GRBs) in the ~1 TeV to 100 TeV energy range. Detection of GRBs at different energy thresholds is key to defining and disproving progenitor and emission models. In this thesis the scaler analysis method is exploited by grouping and summing rates every second from every functioning photo-multiplier tube (PMT) in the pond and looking for statistical excess signal around the time of a GRB over background. The catalog used includes GRBs in the field of view of Milagro between 2001 and the present. No statistical significance was found.

Section 1

Introduction

1.1 Gamma-Ray Bursts

Gamma-ray bursts, or GRBs, were first detected by a group of Los Alamos scientists in 1973[1]. Using the classified VELA satellites that were originally built to detect nuclear weapon explosions in the atmosphere, the scientists were able to conclude after some work that the sources of spontaneous gamma-ray radiation were of cosmic origin. Many theories about what created these bursts were thought of, and the distance to the bursts was still under question. Since then, many earth and space based observatories have been built to learn more about this phenomenon and much work is still being done to understand them.

One of the more recent of these was the Compton Gamma-Ray Observatory that housed the BATSE GRB detector. After releasing its catalog of 2704 bursts detected[2], it was realized that the bursts were isotropic in the sky as shown in Figure 1.1. There was also evidence there were two types of bursts, short and long duration, shown in Figure 1.2. The BeppoSax satellite was the first to detect an X-ray afterglow component to a GRB in 1997, which allowed for higher angular resolution than gamma-ray observations.

[1] Klebesadel, R. W., Strong, I. B. & Olson, R. A. (1973) *Astrophys. J. Lett.* **182**, 85-88
[2] http://www.batse.msfc.nasa.gov/batse/

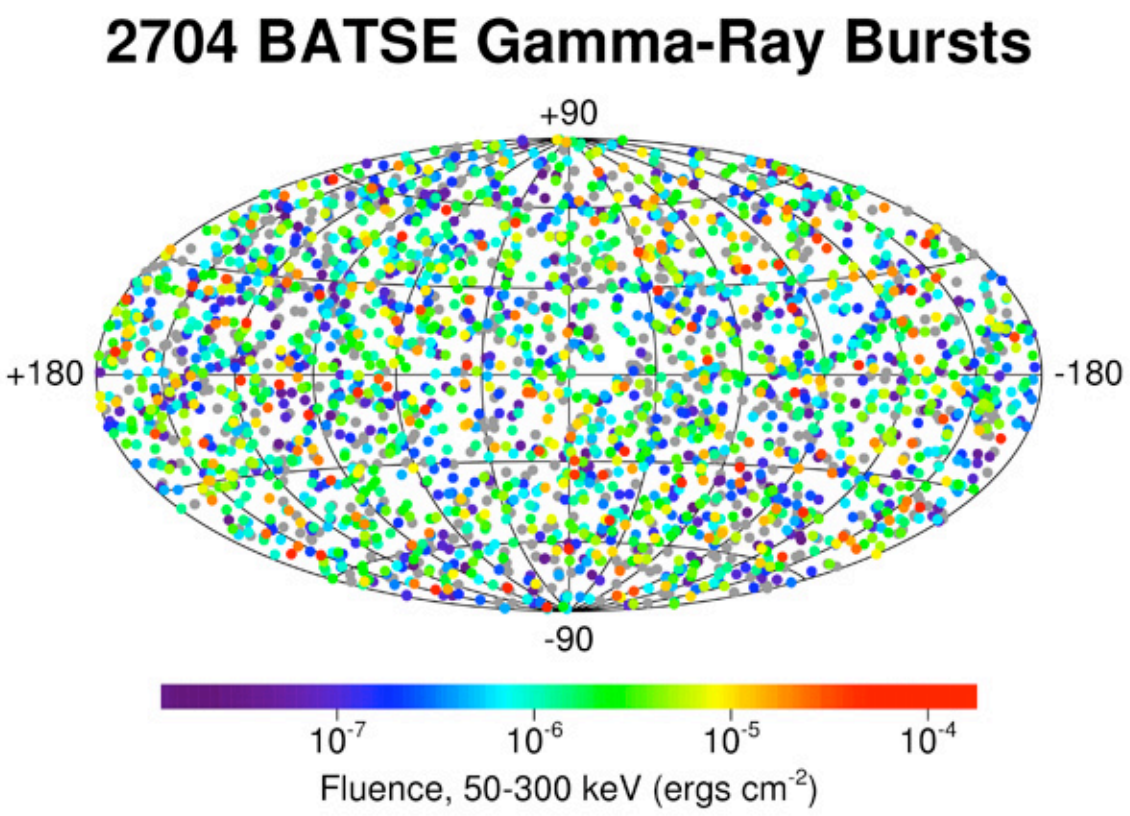

Figure 1.1: BATSE sky map of 2704 GRBs clearly shows their isotropic characteristic. Figure is from BATSE web page. http://www.batse.msfc.nasa.gov/batse/

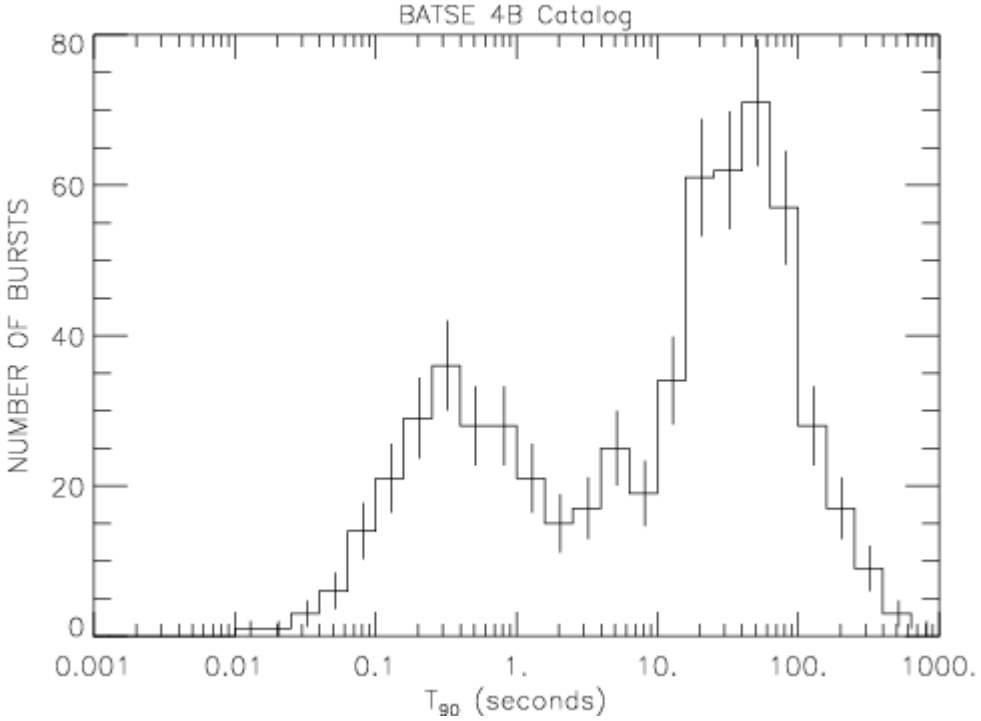

Figure 1.2: BATSE histogram of burst duration clearly shows a double peak distribution, evidence of short and long duration bursts. Figure is from BATSE web page.

Due to this, a host galaxy to the GRB was resolved and measured at $z > 0.835$ (Metzger et al., 1997), solid evidence that the majority of bursts were at cosmological distances.

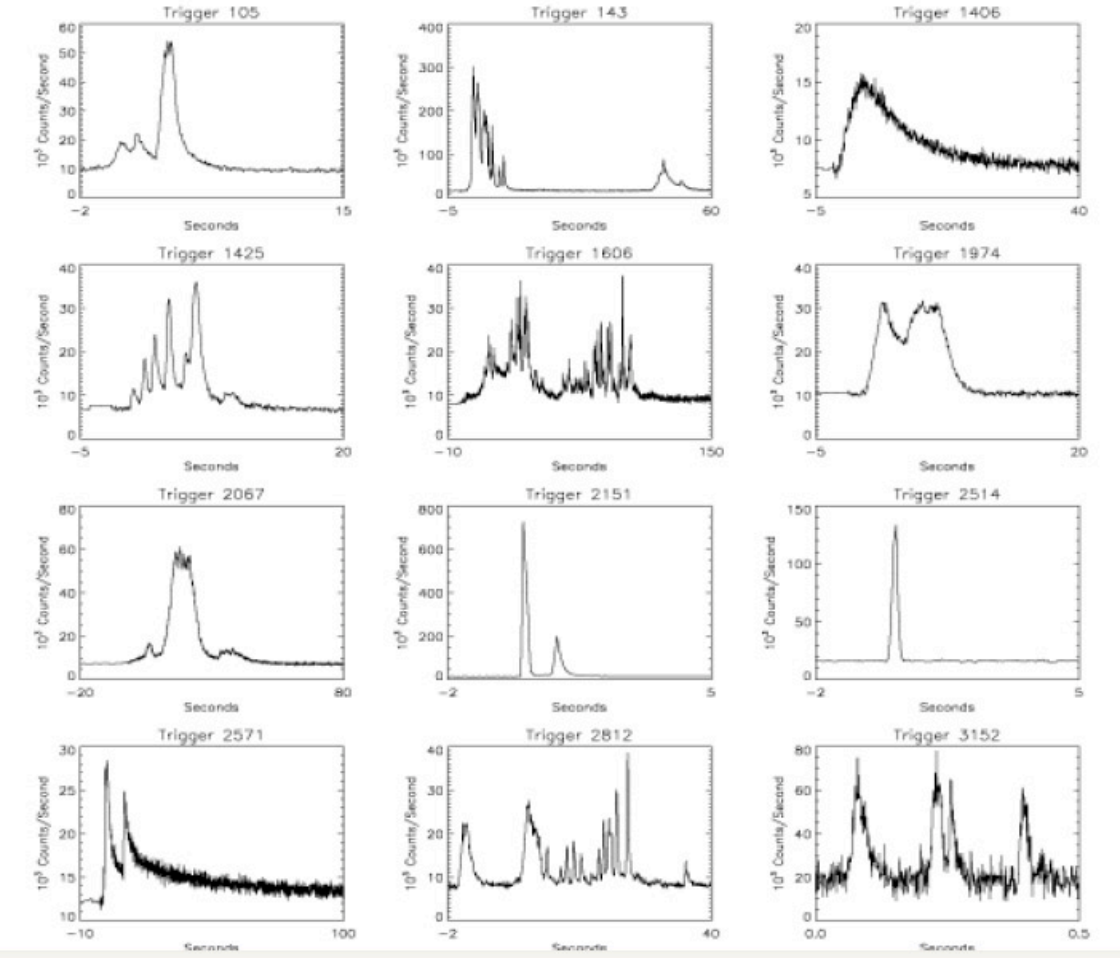

Figure 1.3: GRB light curves are varied, complex, and unique. Credit J. Bonnell, NASA/GSFC

Many theoretical models still exist about the origin of GRBs, due to the difficulty of detection at high angular and energy resolution and the varied, complex light curves that they exhibit, each unique to itself, as shown in Figure 1.3. Experiments typically run within a narrow energy band and much of the mathematics depends on accurate energy measurements and energy progression. Space-based experiments typically cover lower energy gamma-ray detection at very good angular sensitivity, although with a small field of view. Ground based detection generally covers a higher energy range, but with poor angular resolution.

1.2 Milagro

Milagro is a ground-based air-shower gamma-ray detector located near Los Alamos, NM. It is a 5000 m^2 water tank Cherenkov detector and is situated 2630 m above sea level. Housed in the water are approximately 720 photo-multiplier tubes (PMTs) sensitive to the single photon level of optical energy in two layers. The top of the pond is covered completely to keep any light from entering the water. It is a VHE (Very High Energy) cosmic ray detector of showers with energy ~ 1 TeV.

Detection of cosmic gamma rays on the ground is based on the initial gamma ray interacting when hitting the atmosphere and creating an electromagnetic, or E-M, shower that reaches Milagro. A diagram of an E-M shower can be seen in Figure 1.4. The particles that reach Milagro pass through the cover and emit Cherenkov radiation in the visible and near UV photon energy band. The PMTs detect the low energy Cherenkov photons and output a digital read-out of hits.

A gamma ray generates a different shower than a cosmic proton. A proton generates a chaotic nucleonic core as well as more muons that reach the ground before decaying, resulting in a fragmented, wider, and more random shower than a gamma ray. The muons play an important role in detection, as these particles tunnel further in the water as they emit Cherenkov radiation, while the E-M component does not reach as far. Due to this, the PMTs at Milagro are placed at two different depths, illustrated in Figure 1.5. The top layer is for E-M shower component detection, while the deeper layer is called the muon layer.

If the cosmic ray entered the atmosphere at a 0^o zenith angle, then the particles created from the E-M shower would reach the surface very close to the same time. However, most gamma rays hit at varying zenith angles but reconstruction is possible to better than 1 degree angular sensitivity. This is possible by accurately measuring time differences throughout the pond as the shower hits and is detected. However, in this method there must be a minimum number of hits detected before accurate reconstruction can take place. The time sensitivity of hits on the PMTs is good to the nanosecond making subtle time differences between PMT hits within a shower event detectable and the method of reconstruction possible.

The number of hits in the PMTs is correlated to the energy of the original cosmic ray. It is calibrated through Monte Carlo simulations by simulating a high-energy gamma ray event in the sky and using analysis programs to output an expected number of hits.

However, there is another method of event analysis using scaler data. Instead of reconstructing events on an event-by-event basis, scaler analysis involves summing the hits of each PMT each second and calculating excess signal from background. What is lost in directionality is gained by higher sensitivity measurements for low energy events. This data processing technique is outlined in detail in the next section.

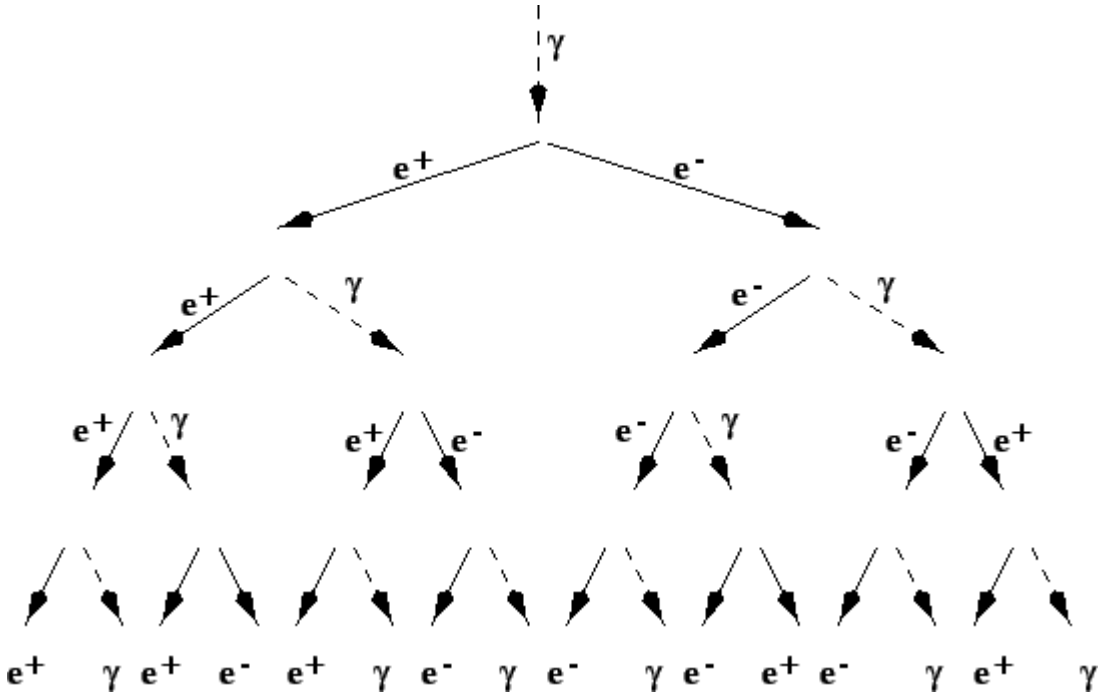

Figure 1.4: An electro-magnetic shower begins when the initial gamma-ray of sufficient energy interacts with the upper atmosphere, creating an electron-positron pair. These particles then continue to interact and create electrons, positrons, and other gamma-rays each of lower and lower energy. If the energy of the original photon is enough, then the E-M particles can be detected on the ground.

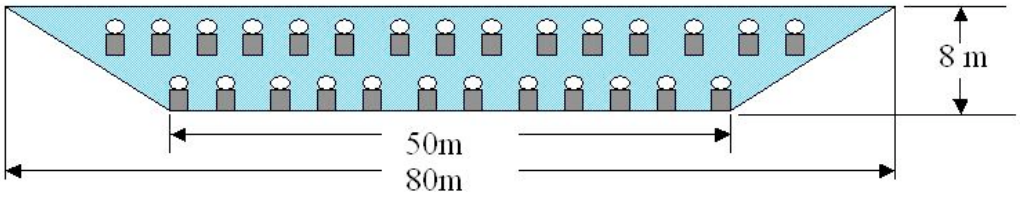

Figure 1.5: A simple illustration signifying the two-layer concept of Milagro. Each layer is hit a different amount depending on the particles present in the shower.

Recent improvements to Milagro have included adding outrigger water tanks (finished in Fall 2002) around the perimeter of the experiment, essentially increasing the surface area and therefore the sensitivity of the experiment, especially for higher energy events or events where the shower center does not hit the main pond. An aerial representation is found in Figure 1.6. The tanks house the same PMTs found in the main Milagro pond, are filled with water, and work the same way as miniature Milagro ponds.

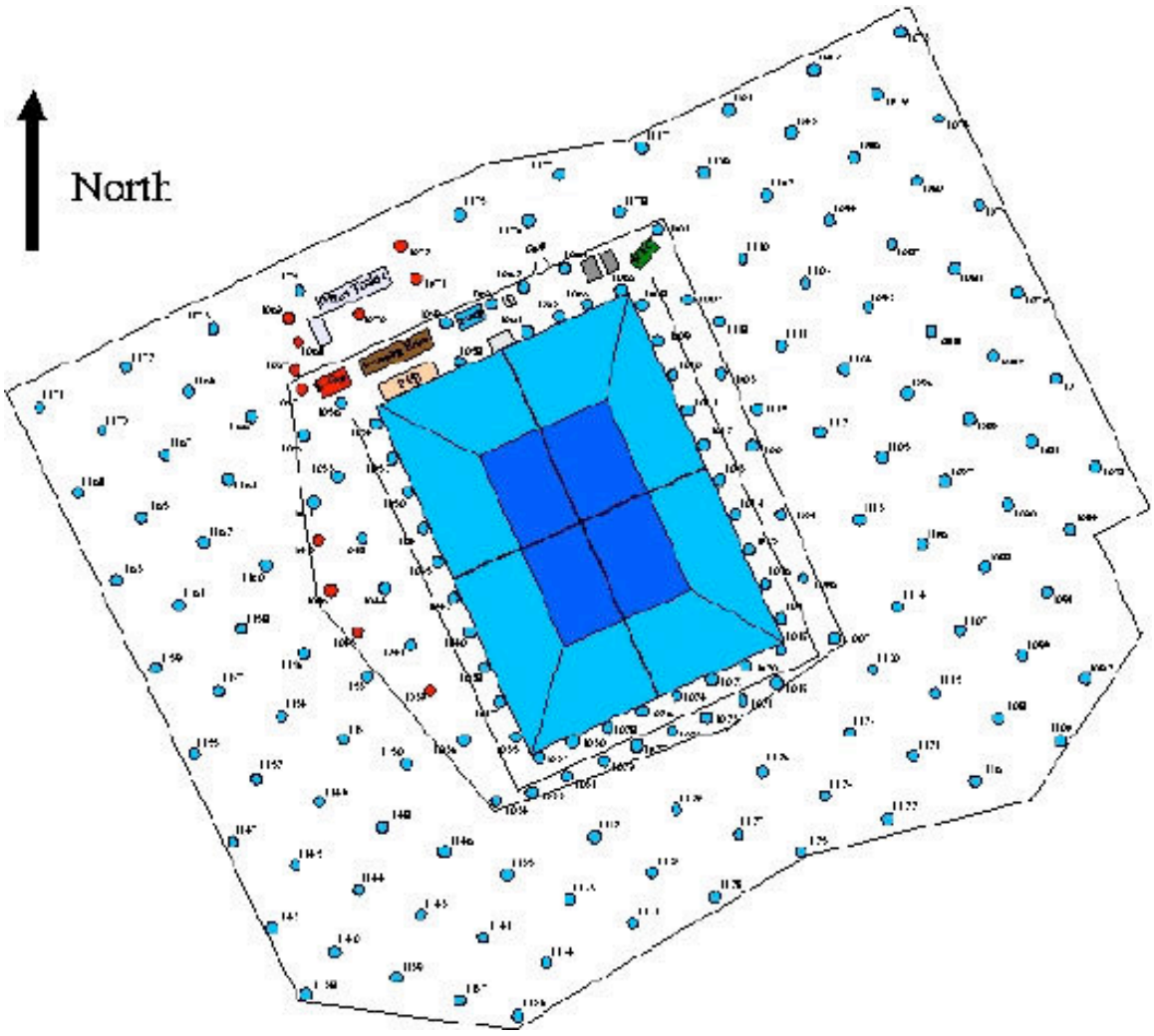

Figure 1.6: Aerial representation of Milagro with additional outrigger water tanks. Source: http://www.physics.nyu.edu/~am3/Milagro.html

Chapter 2

Scaler Analysis

2.1 PMT Groupings

The PMTs in the Milagro experiment are grouped together into two layers, the shallow air-shower array and deeper muon array, which are then split into two thresholds, low and high. With the additional outrigger array, which became operational in Fall 2002, which is also split into low and high thresholds, Milagro has 6 unique groupings of tubes. The low threshold corresponds to single-photon detection sensitivity or more, and the high threshold's sensitivity is approximately 5 photon-electrons or more. The analysis of bursts before the outriggers were operational in Fall 2002 will include the four remaining arrays, low/high air array and low/high muon array. For the recent bursts, low/high outrigger array will be included.

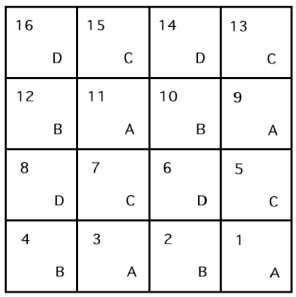

Figure 2.1: Scaler groupings into channels A, B, C, D within a block of 16 PMTs. Credit: R. Atkins, et al. Astrophysical Journal 583 (2003) 824-832

Within an array, PMTs are grouped together into OR channels. The air shower low is groupings of 8 PMTs, while the air-shower high and muon low/high arrays are groups of 16 PMTs. The layout of groupings is shown in Figure 2.1. PMTs are grouped into one of four channels (A,B,C,D). For the air-shower low which is groups of 8, A and D are OR-logically combined, as are B and C. For the rest of the arrays, the block of 16 PMTs is grouped into one OR channel.

During operation, the OR'ed groupings read out data each second. Within the OR group, data is collected in clock cycles of 16 seconds, with an individual PMT collecting data for 1 second during the 16 second clock cycle. This saves data gathering space and still allows for accurate measurements of the Milagro sky.

The air shower low threshold has 58 OR'ed groups, the air shower high threshold has 29 OR'ed groups, the muon shower low threshold has 17 OR'ed groups, the muon shower high threshold has 18 OR'ed groups, and both the outrigger low and high threshold has 11 OR'ed groups.

It is noted that the examples in this section pertain to a special case of cosmic gamma-ray influx, the SGR1806-20 that occurred on December 27, 2004. It was a main focus of study of my research work for the past year due to being in Milagro's sky and its high fluence of gamma-rays. The soft gamma-ray repeater radiated in gamma-rays for a fraction of a second twice as much energy as the sun radiates in a quarter million years[3].

[3] K. Hurley, S.E. Boggs, D.M. Smith, et al., sub. To Nature, astro-ph/0502329

2.2 OR Channel Exclusion

In any experiment, there are bound to be interruptions or faulty equipment breaking up the data-gathering stream. Milagro is no exception, and with a pond of 730 PMTs, there is a good chance a handful will give incorrect readings, the main culprit being water leaking into the PMT housing and shorting the circuitry. This can cause erratic behavior before failure. However, since we are working with OR channels, the groupings of tubes we need to analyze is much less than the total number of PMTs and can be done through a computer program. We developed a systematic mathematical approach to searching for deviant OR channels which I will outline here. First, figures 2.2 and 2.3 display count rates of a functioning and faulty OR channel. Remember, since we're dealing with OR channels, not every tube in that OR group is faulty, however if that OR channel is excluded then every tube in that OR group is excluded from statistical analysis.

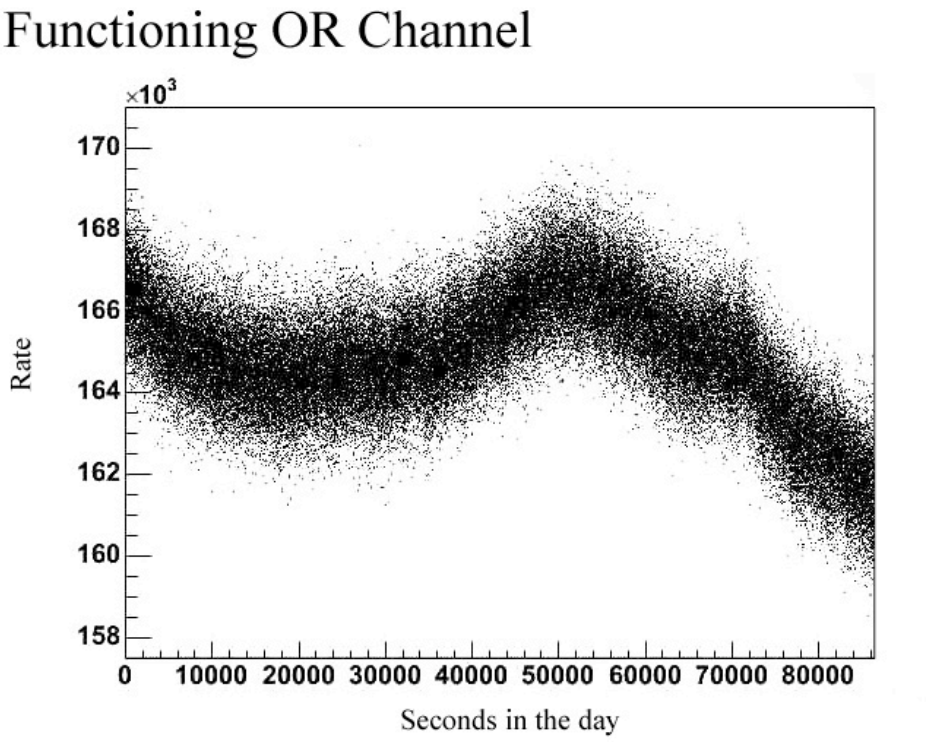

Figure 2.2: OR channel from Julian date, 2453366.5, date 12-27-2004. The rate trend seen is a result of varying atmospheric pressure and temperature changes throughout the day at Los Alamos, NM. This is an example of an OR channel included for statistical analysis.

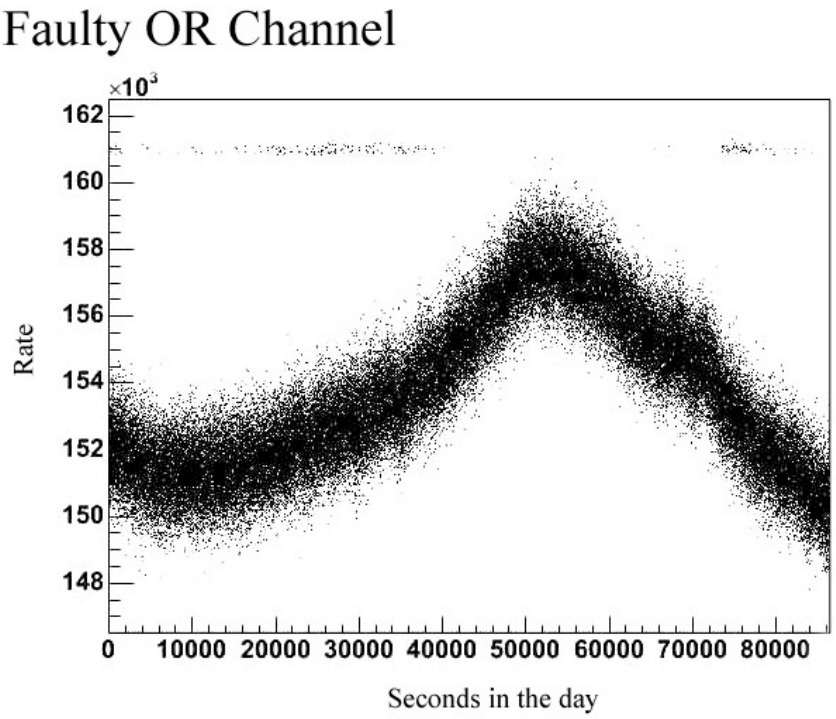

Figure 2.3: OR channel from Julian date, 2453366.5, date 12-27-2004. The rate trend seen is a result of varying atmospheric pressure and temperature changes throughout the day at Los Alamos, NM. This is an example of an OR channel chosen to be excluded from statistical analysis. It can be visually seen that within this OR channel, one or more PMTs is occasionally maxing out its signal threshold, resulting in some seconds of data lying in a line at a rate ~ 1.61×10^5.

Outlined here are the steps to determine statistically faulty OR channels. Removing these channels allows the experiment to statistically run at more sensitivity than including all channels. The method is based on statistical theory for determining the highest sensitivity of the experiment based on the RMS distribution of OR'ed channels.

First, the root-mean-square deviation (RMS) of the average counts in an OR channel is calculated using eq. 2.1. The average rate, 'x' is calculated by summing the rates from each OR'ed group over the 10-day period around a burst being analyzed and dividing by the number of readouts the OR'ed groups gave within the time period (due to slight time drift between the data acquisition system clock and GPS clock, OR groups do not read out exactly every 1 second but close to it).

Eq $$RMS = \sqrt{(\langle x^2 \rangle - \langle x \rangle^2)} \qquad (2.1)$$

The RMS threshold which functioning tubes must be below is given in eq. 2.2. The square of the average RMS, RMS^2_{ave}, is calculated by taking the RMS found in eq. 2.1

Eq $$RMSThreshold = \sqrt{[(2 - \frac{1}{total}) RMS^2_{Ave}]} \qquad (2.2)$$

and summing their squares within each array, then dividing by the number of OR'ed groups within the array. The number of OR'ed groups used in the previous sentence is also 'total' in eq. 2.2. Equation 2.2 is derived by deciding whether adding an OR channel increases the sensitivity of the experiment, or introduces more noise that hinders sensitivity (even if there is some signal in a noisy channel, the experiment will be more sensitive if removed due to these conditions). The RMS threshold is the "breaking point" at which, if an OR channel's RMS exceeds, then by excluding it the new collection of OR channels used in the analysis will be more sensitive to signal than before exclusion.

Now, with the RMS threshold calculated for a particular array, the RMS of each OR'ed group within that array is compared to this threshold and if it is greater than the threshold, the OR channel is noted for exclusion. If no OR'ed groups are found to exceed the RMS threshold, then each channel is within statistical bounds to not be noisier than the others. However, if OR channels are found to exceed the threshold RMS, then they are excluded and the whole process is run again to get a new RMS threshold value to test

against the new group of OR channels. In other words, it is an iterative process until none of the OR channels exceed the RMS threshold for their groupings. Once that occurs, the excluded channels are noted and removed from statistical analysis.

Figures 2.4 and 2.5 demonstrate this process. Figure 2.4 is a histogram of OR channel's RMS for the entire low-threshold air shower array for the Julian day 2453366.5, date 12-27-2004. Figure 2.5 is a histogram of the same array for the same day, but with the noisy OR channels excluded. As can be seen, the higher RMS channels have been excluded using this automated process and the channels left are below their calculated RMS threshold value.

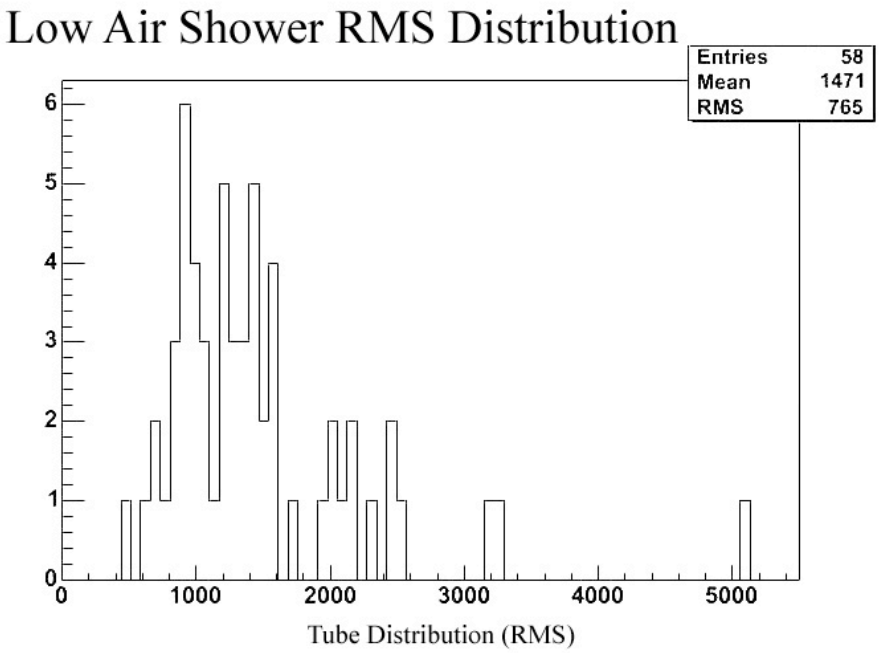

Figure 2.4: Low air shower array OR channel RMS histogram with no exclusions, from Julian date 2453366.5, date 12-27-2004.

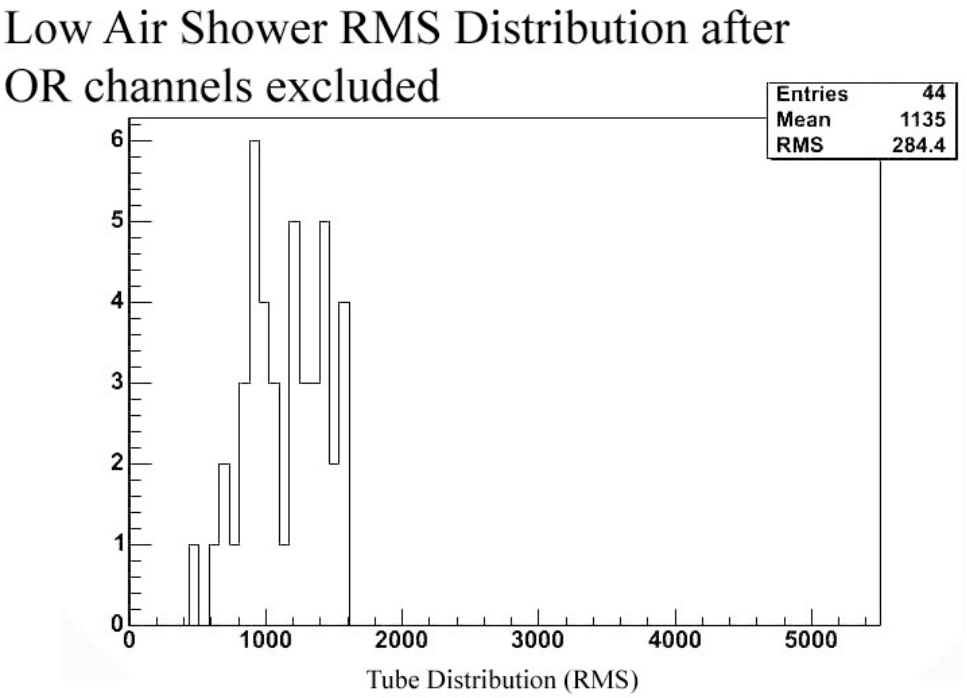

Figure 2.5: Low air shower array OR channel RMS histogram after exclusions, from Julian date 2453366.5, date 12-27-2004. 14 OR channels were excluded, all with RMS greater than the RMS threshold calculated, around 1650.

The calculations outlined in section 2.2 are done independently for each of the six arrays, the low/high air shower, low/high muon, and low/hi outriggers. After we've excluded the noisy channels, we're ready to analyze the data and look for statistically significant excess signal during the time of a GRB. This is outlined in section 2.3.

2.3 Calculating Significance

Because this thesis is focused on doing scaler analysis, there are no spatial correlations to calculate, only the time of the burst and duration are relevant. The spatial coordinates are used to see if the GRB was in the field of view of Milagro at the time of the burst. It is assumed that events detected in the background region are random in nature, and arise from charged cosmic rays (protons) that are randomized from the galactic magnetic field.

To calculate excess signal, first the time around the burst is broken into two intervals, signal and background, as shown in Figure 2.6. The signal interval begins at the time the GRB is initially detected, and ends at the GRB burst time + GRB duration. In other words, it is the time in the day that the GRB is radiating, as seen from other GRB detectors. The background interval is split into two, one before the signal interval and one after. Both are the same length, and equal 5 times the signal interval length (essentially 5 times the GRB duration), and are placed before and after the signal interval. Figure 2.7 shows the low threshold air shower array summed OR channel rates signal and background intervals. The plot is analyzing SGR1806-20, the soft gamma-ray repeater mentioned in the previous section, which had a start time of 77426 UT seconds and duration of 2 seconds. The red points correspond to the signal interval, while the white correspond to the background interval.

Figure 2.6: A simple visualization of how the intervals are cut in the time axis. The signal interval corresponds to the GRB duration and time in the day. The background intervals make up the time around the signal interval and equal 5 times the length of the signal interval.

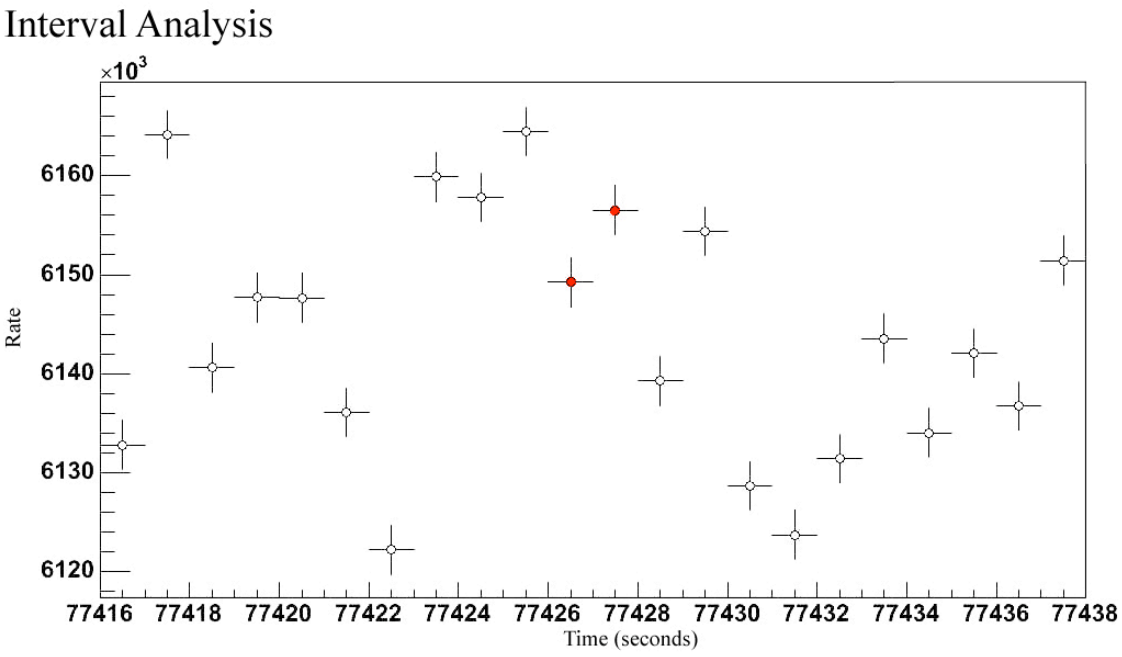

Figure 2.7: Low threshold air shower summed rates of functioning OR channels analysis of SGR1806 during Julian date 2453366.5, date 12-27-2004. The red points correspond to the signal interval. The white points correspond to the background rates around the burst. The background interval is 5 times the length of the signal interval.

First we calculate the average rate and RMS of the signal and background intervals. The RMS is calculated using eq 2.3. This is done individually for the six different arrays. The rates are summed to 'n', or the number of seconds of the interval.

Eq
$$RMS = \sqrt{\left(\frac{\left(\sum^{n} rate^2\right)}{n} - \frac{\left(\sum^{n} rate\right)^2}{n}\right)\left(\frac{n}{(n-1)}\right)} \qquad (2.3)$$

The significance is calculated by taking the difference of the average rates of the signal and background and combining the errors to get the error on the difference, and comparing it to see how consistent that difference is with the null hypothesis. This is shown in eq 2.4. The error on each average rate is given by RMS / $(n)^{1/2}$.

Eq
$$\sigma = \frac{\frac{\sum^{n_1} rate_{signal}}{n_1} - \frac{\sum^{n_2} rate_{bkg}}{n_2}}{\sqrt{\frac{RMS_{signal}^2}{n_1} + \frac{RMS_{bkg}^2}{n_2}}} \qquad (2.4)$$

For GRBs with duration 1 second, the error on the signal is set to 0.

As a test to see whether the method was correctly calculating significances for the random sky, the procedure was run for random intervals and the significance was plotted in a histogram. Roughly 38,000 intervals were scanned and significances calculated, and the low air shower array values were added to a histogram, which is shown in Figure 2.8. It is noted that none of the random intervals overlap each other.

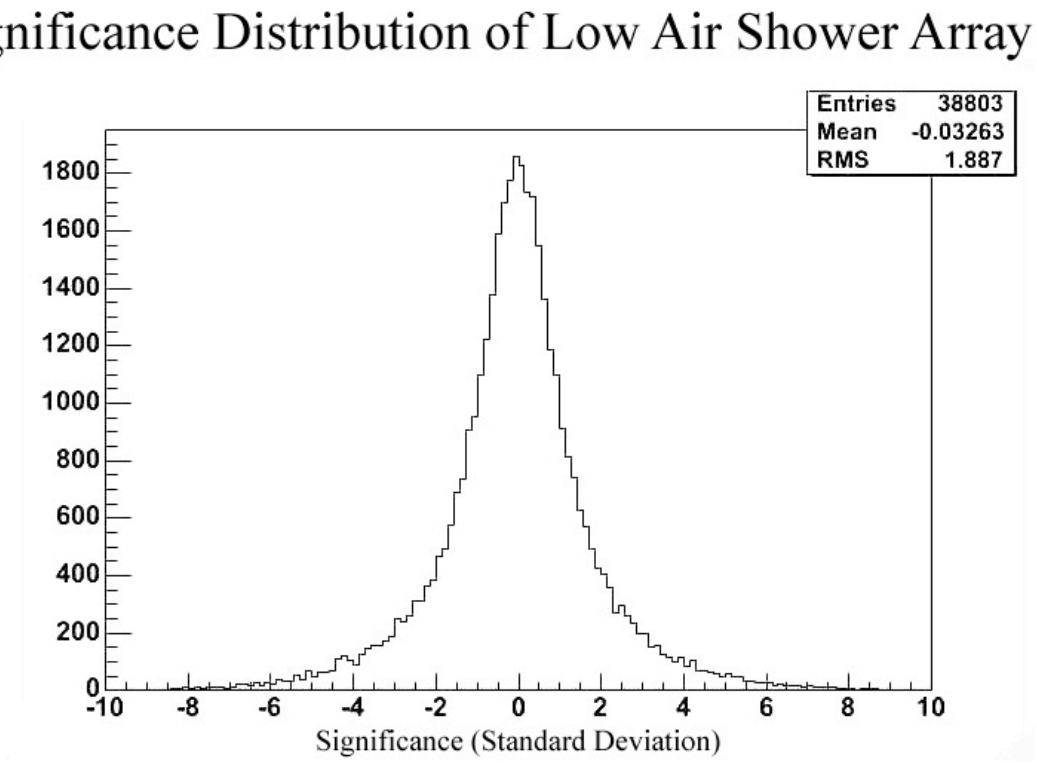

Figure 2.8: Significance distribution for the low air shower array of 38803 intervals calculated at random, with no overlap. The mean and RMS of this distribution is shown in the upper right.

The mean is as expected, near zero, but the RMS is not the expected value of 1. Although resembling a symmetrical bell curve, it is not the expected Gaussian distribution because its standard deviation is closer to 2. Therefore, there are systematic behaviors in the counting rate that aren't being accounted for. For example, the scaler count rates are dependant on atmospheric temperature and pressure, and on the counting house temperature. These nuances are more difficult to fix in general, so a simpler method is outlined in the next section that details how to re-normalize the calculated significance values and get accurate confidence levels.

2.4 Re-normalizing Significance

The method of renormalization is the boot strap technique of taking the methods outlined in section 2.2 and 2.3 only for random data sets of the same burst duration the confidence level is measuring, and tallying the significances calculated (essentially, Figure 2.8 is the histogram from one such run with 38,000 data samples). The number of times a random data set gets a significance higher than the significance of the GRB time divided by the number of samples gives the confidence level. This is done for each array, and is shown in eq. 2.5.

Eq

$$Confidence\ Level = \frac{N_{random\,\sigma > GRB\,\sigma}}{N_{total\ samples}} \tag{2.5}$$

The accuracy of this method is determined by how many individual (non overlapping) data samples can be done realistically. This is not determined by computing power, as we have plenty, but by the experiment on-time. However, that is limited by the individual PMT functional behavior, which becomes apparent by the number of OR channel exclusions within a longer period of time. A limit of a roughly 10 day period is reasonable with respect to accuracy of the confidence measurement and is within bounds of reasonable PMT tube behavior (the number of OR channel exclusions is reasonable). Also, the number of data samples depends on the burst duration. A 10 day period grants roughly 39,000 samples for a 2 second burst duration (intervals of 10 – 2 – 10, therefore 22 second total sample length) while only 1,500 samples for a 50 second burst duration (intervals 250 – 50 – 250, therefore 550 seconds total sample length). However, as most of the bursts being analyzed are not very long duration, with only a few > 100 seconds, the confidence levels are accurate to at least 1%.

After the confidence level is calculated, a re-normalized significance can be calculated using the complementary error function and the confidence level in the usual manner, eq. 2.6.

Eq $$Confidence = \frac{1}{2} erfc \frac{\sigma}{\sqrt{2}} \quad (2.6)$$

The factor of one half is needed because the method for calculating the confidence level is only counting the error of the right tail of the Gaussian distribution, while the complementary error function calculates for both tails. To get the significance from eq. 2.6, an inverse complementary error function is needed. A sufficient approximation for such a function was used, credit to http://www.codecogs.com/d-ox/maths/special/errorfn_inv.php website and the GNU open-source library. When testing the function on standard deviations of 2 and 3, the approximation of the standard deviation is good to 4 decimals.

Section 3

Data Sample and Results

3.1 GRB Catalog

Pablo Saz Parkinson created the GRB catalog used for the analysis outlined in this thesis. The scaler analysis doesn't take spatial coordinates into consideration, but when choosing which GRBs to find correlations with, it is the only consideration. Milagro is a ground-based observatory so its RA and DEC coverage changes continuously throughout the day. The list includes bursts in Milagro's field of view within a 45^{o} zenith angle, from January 2000 to May 2006. It is presented in Table 3.1. The rate of bursts since December 2004 has substantially gone higher because of detection by the Swift GRB satellite. Also included is the special case of the SGR1806-20 that was discussed earlier in the text. This SGR radiated a short peak of gamma-rays on December 27, 2004 at 77426 UT seconds, duration 2 seconds. The Julian date is truncated by subtracting 2450000.5 from the Julian date. Duration is in seconds, and zenith angle is in degrees.

GRB Catalog Years 2000 - 2005

GRB	Julian Date	UTC	Duration	Zenith θ
000212	1586	81065.2	8	2.21
000226	1600	13909.4	10	31.5
000301C	1604	35497	14	37.6
000302	1605	10225.1	120	31.9
000317	1620	77953.8	550	6.39
000330	1633	75449.4	0.2	30.0
000331	1634	85421.8	55	38.3
000408	1642	9348.2	0.2	31.1
000615	1710	22704	10	39.0
000630	1725	1853	20	33.2
000926	1813	85773	25	15.9
010104	1913	62489	2	19.8
010220	1960	82267	150	27
010613	2073	27234	152	24.7
010921	2173	18950.6	24.6	10.4
011130	2243	22775.7	83.2	33.7
011212	2255	14642	84.4	33
021104	2582	25262.9	19.7	13.3
021112	2590	12495.9	7.1	33.6
021113	2591	23936.9	20	17.6
021211	2619	40714.0	6	34.8
030413	2742	27277	15	27.1
030823	2874	31960.6	56	33.4
031026a	2938	20143.3	114.2	33.0
031220	2993	12596.7	23.7	43.4
040924	3272	42731.36	0.6	43.3
041211	3350	41507	30.2	43.0
041219a	3358	6138	520	26.9
050124	3394	41403	4	23.0
050319	3448	34278.44	15	45.1
050402	3462	22194.58	8	40.4
050502	3492	8037	20	42.7
050504	3494	28852.5	80	27.6
050505	3495	84141.09	60	28.9
050509b	3499	14419.23	0.128	10.0
050522	3512	21621	15	22.8
050607	3528	33082.8	26.5	29.3
050712	3563	50427.51	35	38.8
050713b	3564	43637.62	30	44.2
050715	3566	81026.42	52	36.9
050716	3567	45363.63	69	30.3
050820	3602	23693.11	20	21.9
051109	3683	4340	36	9.6
051111	3685	21581.5	20	43.7
051211b	3715	79544	80	33.3
051221	3725	6675.61	1.4	41.8
051221b	3725	72200.09	61	25.9

Table 3.1: Credit Pablo Saz Parkinson. GRB catalog of bursts during 2000-2005. Bursts falling within 45 degrees zenith at Milagro are included. Julian date is truncated as described in the text. Duration and UTC are in seconds. Zenith angle is in degrees.

GRB Catalog January – May 2006

GRB	Julian Date	UTC	Duration	Zenith θ
060102	3737	76648	20	39.9 R
060109	3744	60881	10	22.4 R
060110	3745	28877	15	43.0 S
060111b	3746	72943	59	36.5 S
060114	3749	45586.1	100	40.6 S
060204b	3770	52464	134	30.5 R
060210	3776	17929.8	5	43.4 S
060218	3784	12870.97	2000	43.7 S
060306	3800	2950	30	46.2 S
060312	3806	5772	30	43.6 S
060313	3807	726	0.7	46.7 S
060403	3828	47537	25	27.6 S
060427b	3852	85915	0.2	16.4 S
060428b	3853	32079	58	26.6 S
060507	3862	6792	185	47.1 S

Table 3.1 continued: Credit Pablo Saz Parkinson. GRB catalog of bursts for January – May 2006. Bursts falling within 45 degrees zenith at Milagro are included. Julian date is truncated as described in the text. Duration and UTC times are in seconds. Zenith angle is in degrees, and an R in the zenith angle column denotes a rising source, while an S denotes a setting source.

3.2 Results

The analysis program uses the start time of the burst and duration. Scaler cycles run approximately each second, but the values for the bursts can be better accuracy, as seen in the table. If the start time is of accuracy to a fraction of a second, it is entered with the fraction of the second. If the duration is of accuracy to a fraction of a second, it is rounded up to the nearest whole number. If the duration is less than a second, such as 0.2, then a value of 1 second is used. Table 3.2 displays the results of the analysis. Given in the table are the significance calculated after re-normalization for the bursts in Table 3.1 for the 6 arrays. For the bursts before Fall 2002, the low/high outrigger (named OR in the table) arrays are omitted.

Table of Significance of 6 Individual Arrays for GRB list from Years 2000-2005

GRB	Air-Low	Air-High	Muon-Low	Muon-High	OR-Low	OR-High
000212	0.24	-1.28	0.39	-0.58	-	-
000226	-0.42	-2.28	-1.00	-1.57	-	-
000301C	0.04	0.10	0.16	-0.65	-	-
000302	-1.33	-0.48	-1.58	0.05	-	-
000317	0.77	-1.34	-0.74	-1.39	-	-
000330	-0.14	0.78	-0.38	0.42	-	-
000331	0.51	-0.73	-0.33	-0.99	-	-
000408	-1.41	-0.08	1.18	0.32	-	-
000615	-1.90	-1.34	-1.37	-1.73	-	-
000630	0.89	-0.14	0.76	0.61	-	-
000926	-0.91	-0.34	0.03	0.79	-	-
010104	1.50	1.84	1.64	0.14	-	-
010220	-1.12	0.95	-1.42	-1.86	-	-
010613	0.83	0.39	1.24	0.22	-	-
010921	-1.03	-1.24	-1.47	-1.09	-	-
011130	-1.26	-1.59	-1.32	-1.64	-	-
011212	0.38	-0.80	-1.66	-1.45	-	-
021104	0.58	-0.13	1.71	2.59	0.45	-0.63
021112	-0.72	-1.02	0.51	0.76	1.14	1.20
021113	-1.01	-1.45	-0.48	-0.37	0.15	0.16
021211	0.31	0.32	0.95	1.32	-1.29	0.15
030413	-1.67	-1.37	-1.52	-1.15	-0.02	1.01
030823	-0.53	0.84	0.22	-0.02	-0.24	-0.69
031026a	-1.29	-0.31	-0.84	0.25	-0.36	1.27
031220	0.34	0.90	0.31	0.66	-0.47	0.14
040924	-0.52	-0.59	-0.46	-0.44	-1.92	-1.59
041211	1.40	2.30	1.75	-0.64	0.38	-0.40
041219a	1.05	0.60	-0.33	0.55	0.98	0.53
050124	-0.62	-0.50	0.10	0.50	1.10	0.62
050319	1.23	0.71	0.22	0.19	0.75	0.85
050402	-1.01	-1.53	0.04	1.49	0.20	0.16
050502	-1.12	-0.87	-1.19	-1.09	-0.01	-0.99
050504	0.03	0.67	0.04	0.15	-0.36	-0.85
050505	-0.56	-0.23	-0.59	-0.35	0.90	1.62
050509b	-0.46	-0.91	-1.94	-1.29	-0.54	0.15
050522	-0.15	-0.26	-0.51	-1.52	1.27	2.05
050607	1.02	0.98	0.34	0.37	0.42	1.80
050712	0.47	0.93	-0.86	-0.63	1.51	-0.16
050713b	0.20	0.23	-1.21	0.03	1.38	0.37
050715	-0.38	-0.41	-0.78	-1.18	1.17	1.31
050716	0.29	0.28	-0.16	0.14	0.44	0.81
050820	-0.35	0.83	-0.84	-0.21	-0.56	0.42
051109	1.03	0.69	-0.58	0.25	0.80	2.50
051111	0.10	-0.72	-0.26	-0.48	0.52	0.63
051211b	0.46	0.56	-0.01	0.07	0.27	0.82
051221	0.6	0.32	0.28	-0.73	-1.32	0.02
051221b	-0.99	0.16	-0.29	-0.75	-0.58	-0.20

Table 3.2: Re-normalized significances calculated on GRB list found in Table 3.1 for years 2000-2006. Outrigger low/high (named OR in table) is omitted for bursts before fall 2002.

Table of Significance of 6 Individual Arrays for GRB list from Year 2006 Jan - May

GRB	Air-Low	Air-High	Muon-Low	Muon-High	OR-Low	OR-High
060102	1.16	1.16	0.86	0.88	-1.57	1.49
060109	-0.80	-0.25	-0.52	-1.13	-2.74	-1.63
060110	-0.96	-1.46	-0.92	-0.25	0.59	0.61
060111b	-0.17	0.13	0.44	0.68	2.12	-0.50
060114	-0.22	-0.99	0.14	-0.88	0.04	-0.28
060204b	0.26	1.67	0.59	0.90	1.32	0.05
060210	-0.59	-0.29	-1.33	0.06	-0.33	-0.26
060218	-0.57	-0.50	-0.50	-0.30	-0.43	-0.30
060306	1.18	0.49	1.01	2.10	-0.46	0.13
060312	0.02	0.77	-0.60	-0.74	0.74	1.75
060313	0.58	0.74	-0.32	-0.55	-0.02	-0.68
060403	-0.33	0.25	-0.13	0.69	1.72	-1.38
060427b	0.38	0.29	0.06	-1.07	0.17	1.08
060428b	-1.03	-1.04	-0.25	-0.78	-0.58	-0.54
060507	0.09	0.43	0.41	0.72	-0.68	0.19

Table 3.2 Continued: Re-normalized significances calculated on GRB list found in Table 3.1 for year 2006 between January and May.

The SGR1806-20, which is omitted from the tables (as it is not a GRB), has calculated re-normalized significance of 1.96, 2.04, 0.53, 0.11, -0.29, and 0.95 for the air shower low, high, muon low, high, and outrigger low and high, respectively.

To search for signal excess from the GRB list in Table 3.1 as a whole, histograms from Table 3.2 for individual array significances and confidence levels calculated are presented in Figure 3.1 and Figure 3.2. The special case of SGR1806-20 is included as well. The data sample of GRBs is somewhat small, and much smaller than the 39,000 entries for a comparison plot of significance calculated before re-normalization on random intervals of time, Figure 2.8. Still, a visible drift towards positive mean of the distributions or outlier entries at large positive values would be promising of detecting a signal from the scalers. If the distributions look Gaussian, though, then there is no statistical evidence for emission present in the catalog of bursts analyzed as a whole.

Figure 3.1, the confidence level histograms, are included as a proof of principle to Figure 3.2. If the significance distributions are Gaussian then we expect the confidence level histograms to be a flat line with 0 slope between 0 and 100. This expectation is realized.

Confidence Level Histograms for GRB Catalog 2000 – May 2006z

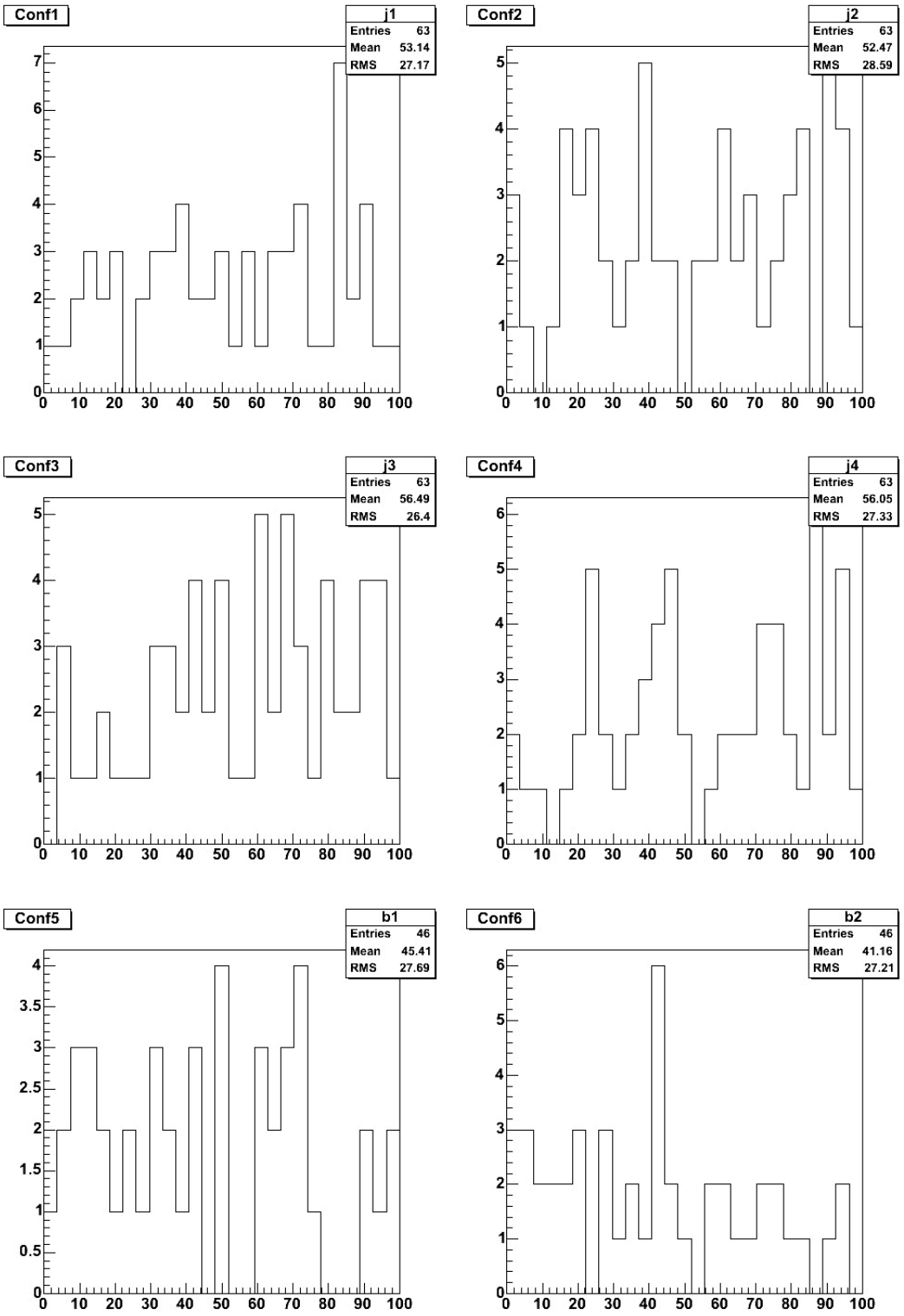

Figure 3.1: Confidence level histograms for air-shower low/high (top left/right), muon layer low/high (middle left/right) and outrigger low/high (bottom left/right) thresholds of the GRB catalog results located in Table 3.1 and 3.2. The confidence measurements were an intermediate step outlined in Section 2, and are shown here as a proof of principle.

Significance Histograms for GRB Catalog 2000 – May 2006

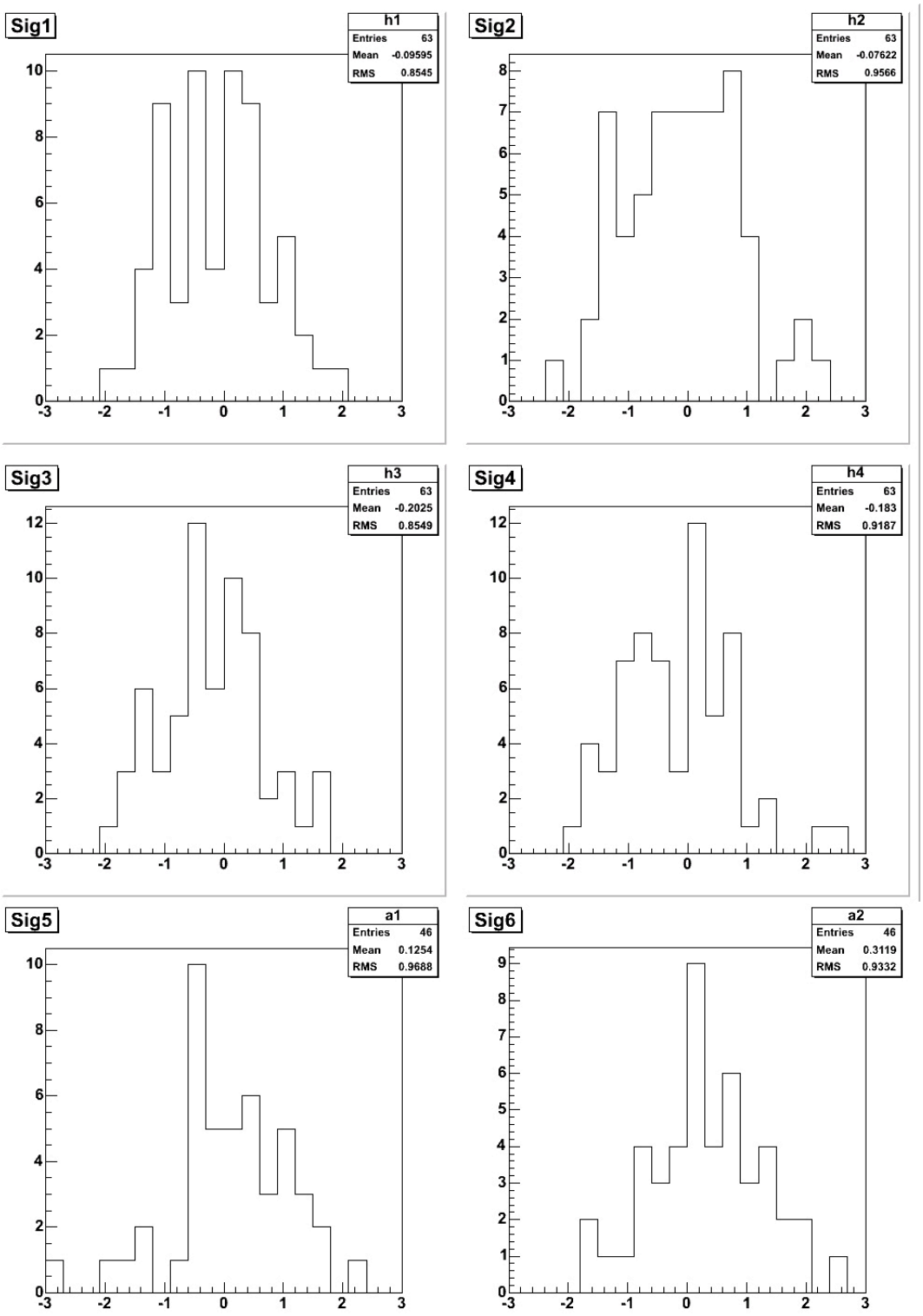

Figure 3.2: Significance histograms for air-shower low/high (top left/right), muon layer low/high (middle left/right) and outrigger low/high (bottom left/right) thresholds of the GRB catalog results located in Table 3.1 and 3.2.

Figure 3.2 shows the six arrays having similar characteristics when calculating excess signal from the GRB table. All have a mean close to 0 and RMS close to 1, however with errors which can be attributed to a small data sample. All six are close Gaussian distributions; in particular, there are no entries standing out at large positive significance. Therefore, no statistical significance of signal over background was found when analyzing the catalog as a whole. When compared to the distribution of significance calculated before re-normalization, Figure 2.8, re-normalization is proof positive in estimating correct significances.

Section 4

Future Direction in Scaler Analysis

My research so far has been working on the analysis of a catalog of bursts from the year 2000 to the present, May 2006. However, recent revelations made by my mentor, Professor David A. Williams, and myself can help expand the scaler analysis technique. One area mentioned in this thesis was the abundance of systematic variables present in the counting rates that manifested in incorrect significance calculations, which were later re-normalized in a computer intensive manner. Looking more closely at data taken during a day reveals short and long term trends in the counting rates, Figure 4.1. This plot is of the air shower low threshold array, removing noisy channels and summing the rest of the OR'ed channels each second.

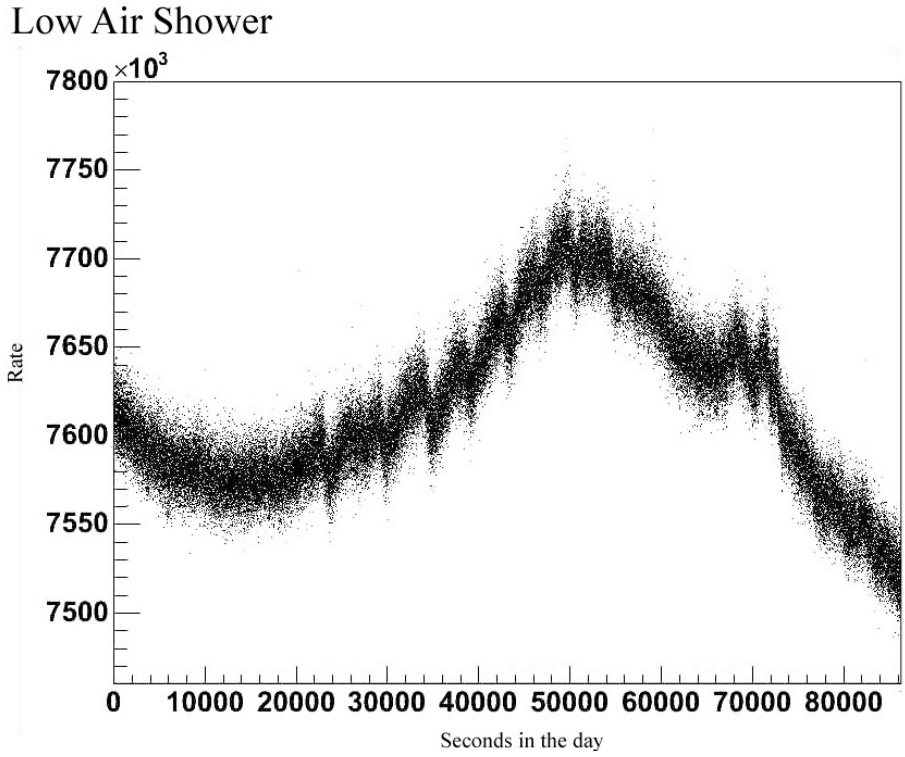

Figure 4.1: Data collected during a day. Noisy OR'ed channels are removed; the rest are summed up each second.

It is evident that there is a short-duration trend of saw-tooth behavior occurring during a good fraction of the day, and a longer duration trend that peaks at 50,000 seconds in the day and oscillates with long wavelength on order of a day. Since most of the GRBs in Table 3.1 are "short" duration, < 100 s, the short trends are more interesting to understand to accurately calculate the significance.

Milagro measures the counting house temperatures using thermocouples and stores the data every couple minutes. By interpolating the data in between measurements, a graph of the counting house temps can be superimposed with Figure 4.1 to see if any trends are present. The air shower counting house data was used, and interpolated, Figure 4.2. An overlay of Figures 4.2 and 4.1 is put in Figure 4.3.

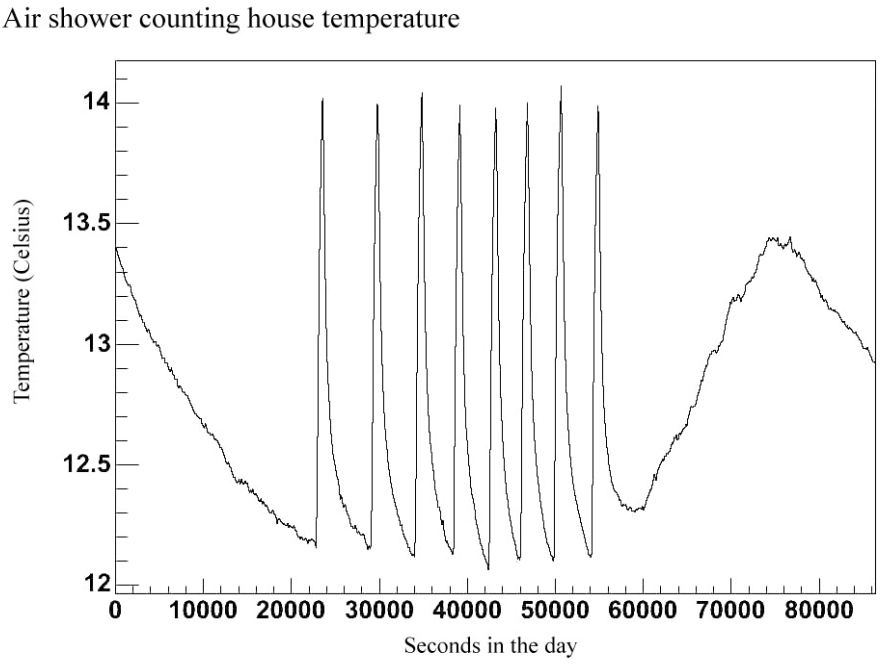

Figure 4.2: Counting house temperature measured in Milagro using thermocouples. Temperature is measured every 2 minutes. The data is linearly interpolated between measurements.

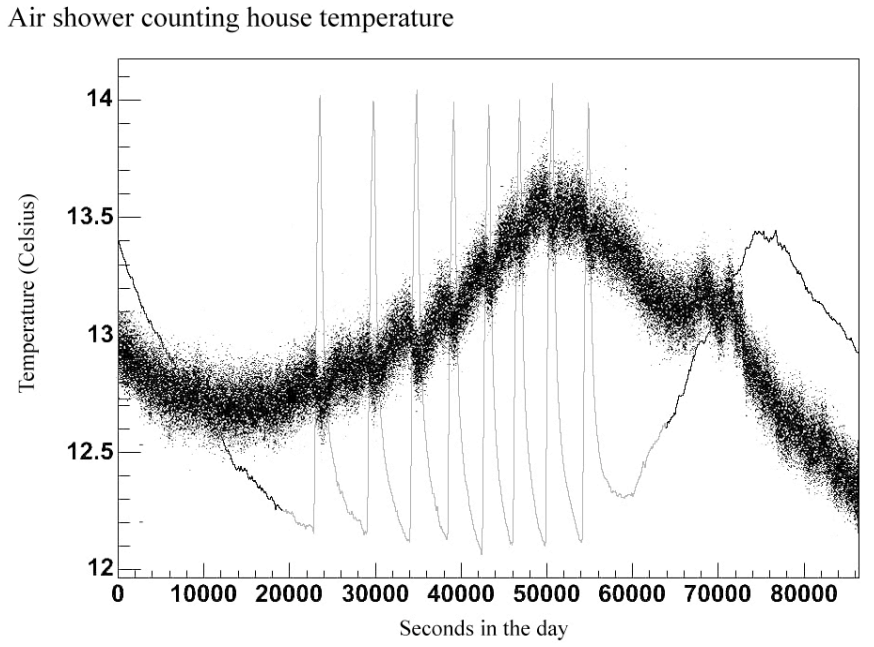

Figure 4.3: Overlap of Figures 4.2 and 4.1. The counting house temperature is artificially faded to make it more visible when comparing with the data.

As noted, there is a strong anti-correlation between the counting house temperature and the short-duration rate trends present in the data between seconds 20,000 and 60,000. This systematic behavior is a good candidate for the significance calculation errors shown by Figure 2.8. There is saw-tooth behavior around 70,000 seconds in the data that is not explained by the counting-house temperature graph. We do not yet have a good candidate for explaining this trend.

Correcting for these systematic behaviors allows us to reduce the intrinsic RMS of the data, therefore allowing the experiment to become more sensitive to signal from a burst. Being more sensitive also allows us to be able to detect bursts of lower gamma-ray fluence.

Another goal is to calculate an upper-limit on the rates for each GRB and use Monte Carlo computer simulations of Milagro's sensitivity to convert those into limits of high-energy gamma-ray flux.

References:

R. Atkins, et al., 2003, APJ 583, 825, Figure 2.1

BATSE web page, http://www.batse.msfc.nasa.gov/batse/

J. Bonnell, Nasa/GSFC, Figure 1.1

K. Hurley, S.E. Boggs, D.M. Smith, et al., *Nature*, astro-ph/0502329

R. W. Klebesadel, Strong, I. B. & Olson, R. A. (1973) *Astrophys. J. Lett.* **182**, 85-88

A. Mincer, et al., Figure 1.6, http://www.physics.nyu.edu/~am3/Milagro.html

P. S. Parkinson, GRB Catalog for Milagro coverage